FACTA UNIVERSITATIS
Series: **Mechanical Engineering** Vol. 22, Nº 1, 2024, pp. 45 - 62
https://doi.org/10.22190/FUME221221011W

Original scientific paper

MODELLING AND SIMULATION OF NONLINEAR DYNAMIC FLOW FIELD AND TEMPERATURE FIELD OF DEPYROGENATION TUNNEL

Yizhi Wang[1,5], Quanmin Zhu[2], Tao Huang[3], Xiaodong Han[4,5], Min Lin[6]

[1]College of Intelligent Science and Control Engineering,
Jinling Institute of Technology, China
[2]Department of Engineering, Design and Mathematics,
University of the West of England, Frenchay Campus, UK
[3]Wuhan Zhongqi Technology Co., LTD, China
[4]College of Computer and Control Engineering, Minjiang University, China
[5]Fujian Provincial Key Laboratory of Information Processing and Intelligent Control,
Minjiang University, China
[6]School of Innovation, Entrepreneurship and Creation, Minjiang University, China

ORCID iDs: Yizhi Wang https://orcid.org/0000-0002-8648-9016
Quanmin Zhu https://orcid.org/0000-0001-8173-1179
Tao Huang https://orcid.org/0009-0004-3752-7153
Xiaodong Han https://orcid.org/0009-0008-5185-8070
Min Lin https://orcid.org/0000-0002-3893-9174

Abstract. *Nonlinear dynamics plays a crucial role particularly in equipment validation of preparation production, validation results of which will significantly influence the results and period of drug registration in drug production processes. In this research, the flow field and temperature field simulation, calculation and analysis are creatively carried out in terms of depyrogenation tunnel, a very popular preparation drying-sterilization equipment in pharmaceutical processes with strong dynamic characteristics. After construction of 3D model of this equipment using Catia and mesh generation applying ANSYS, the computational fluid dynamic (CFD) method and verification of irrelevance method are carried out regarding 6.05 million of meshes to identify the flow velocity model and heat transfer model inside the equipment, to further provide methodology for pharmaceutical process validation and to further optimize the design of control methods. After calculation and simulation, the low-velocity vortices of different sizes inside the hood and the drying chamber are identified, which could cause vials to fall down; meanwhile, vials that are farther away from the outlet receives less heat exchange effect, which would shrink the effective sterilization area, indicating an inadequate validation methodology in pharmaceutical processes.*

Key words: *Depyrogenation Tunnel, Flow Field, Temperature Field, Nonlinear Dynamic Simulation*

Received: December 21, 2022 / Accepted March 10, 2023
Corresponding author: **Min Lin**
School of Innovation, Entrepreneurship and Creation, Minjiang University, No. 200, Xiyuangong Road, Shangjie Town, Minhou County, Fuzhou 350121, China
E-mail: minlin@mju.edu.cn

1. INTRODUCTION

In pharmaceutical engineering, an extremely significant step is sterilization, especially for preparations that directly enter the human body, and its effect is directly related to the safety of people's lives. Physical sterilization has little effect on the activity of drug molecules. Due to this characteristic, in the pharmaceutical industry, physical sterilization is more widely used than chemical sterilization. In physical sterilization, dry heat sterilization is often used, while a dry heat sterilization depyrogenation tunnel is applied as the principal sterilization equipment.

Compared with the far-infrared radiation sterilization method, the implementation process of dry heat sterilization is more controllable in the control of temperature and pressure difference, and it is more in line with Good Manufacturing Practice (GMP) requirements, resulting in higher sterilization quality and efficiency [1, 2]. Consequently, under this premise, the control of the temperature and the control of differential pressure of the sterilization depyrogenation tunnel have become the key control parameters of the equipment. In this regard, Wang and Quan and their groups [3-5] have done research into the optimization of control systems. The optimal design was conducted using methods such as a state space method and type-2 fuzzy control. Moreover, the simulation verification was carried out, and the control effect was theoretically achieved. However, in the actual application process, a series of issues were observed, namely, there was a large difference in temperature rise in the vial due to the uneven distribution of airflow in the depyrogenation tunnel; the abnormal state such as lodging of the dried object placed on the track was caused by the change of wind pressure; during the operation of the depyrogenation tunnel, problems such as energy waste were generated due to the unreasonable artificial regulation. As a result, an in-depth study of the temperature and wind speed distribution in the sterilization depyrogenation tunnel, analysis of the heating characteristics of the dried object, and reduction of energy consumption during the sterilization process of the dried object are of a great theoretical guiding value and engineering application value to improve the production efficiency of the drying of pharmaceutical packaging materials.

Catia software is innovatively applied to model and analyze the representative industrial complex system of the sterilization depyrogenation tunnel, filling the gap in the research on the influence of the equipment structure on the internal flow field.

In addition, ampoules are usually taken as dried objects [6] in the subsequent computational process. However, vials have become popular in recent years for their high error-tolerant rate and injection efficiency [7] and the relevant computational study regarding drying and sterilization processes are yet to be fulfilled. Therefore, taking the common vials as the dried objects, the flow field in the equipment is numerically simulated and studied, which provided a guiding principle for the subsequent optimization and finally the improvement of the control system.

Furthermore, the fluid field and thermal dynamic field are simply considered separately through a computational study for ovens. However, under the specific equipment using hot air for sterilization [3-5], the thermal dynamic field and fluid field are coupled together, which means that when the parameter of velocity is changed, it will influence the thermal dynamic field as well. However, the relevant study is left to be filled.

Taking the drying and depyrogenation process of vials in a depyrogenation tunnel as the research object, this research studied the heat transfer field and fluid flow field and its coupled nature in hot air circulation. Specifically, it studied the problems of uneven flow field of the depyrogenation tunnel and the unreasonable control of the heating process

during the drying and depyrogontation of vials. Using the computational fluid dynamic (CFD) numerical simulation method, the airflow distribution characteristics inside the tunnel and the heating characteristics of the vials were explored, which provided a theoretical basis for improving product quality and reducing production energy consumption and subsequent further modification of control system parameters.

The contributions of this paper are as follows:

- According to the geometric parameters of the depyrogenation tunnel, using Catia software, the three-dimensional physical model of the sterilization section of the depyrogenation tunnel was established, and the resistance characteristic parameters of the porous medium were determined through experiments; the 3D simulation model of the sterilization depyrogenation tunnel was simplified, and mesh-independent verification was carried out. Moreover, the accuracy of the simulation model was verified by using the speed test results of the depyrogenation tunnel in no-load and cold state.
- The internal flow field of the depyrogenation tunnel has been simulated. Through the evaluation index of flow characteristics, the uniformity of the outlet velocity of the depyrogenation tunnel was evaluated.
- After establishing a three-dimensional model of the vials in the depyrogenation tunnel, the transient simulation of the heating process of the vials in the depyrogenation tunnel was performed, and its energy consumption was analyzed and calculated; The influence of process parameters on the heating characteristics of vials, residence time and energy consumption of the depyrogenation tunnel was investigated, and the process parameters were identified.

2. Critical Review

Along with the rapid development of numerical simulation technology, a variety of numerical methods based on theoretical calculation, such as an iterative optimization method [8], finite element method [9], interpolation method [10] and neural network method [11] have been widely used in sterilization process research. However, realization of all these intelligent algorithms needs the support of large base of experimental data, which is to validate the drying and sterilization results of vails taken for experiments rather than to guarantee that every vial has been dried and sterilized as required. Accordingly, it is particularly essential to analyze the temperature field of the heating process of the vial in the sterilization depyrogenation tunnel by using the method of numerical simulation. Meanwhile, the analysis and application in drying and sterilization processing in the pharmaceutical industry using CFD regarding the airflow field and temperature field concurrently is yet to be flourished for the following reasons:

- The influence of thermal transfer to food flavor is under the spotlight due to the development of food industry and market demand rather than the pharmaceutical industry [12]. For example, the local convective heat transfer coefficient of oven is studied using CFD in terms of bread baking process for better flavor and less energy consumption [13-15]; a drying process and its influence to a solvent in terms of can industry is studied using a CFD method [16]; a drying and sterilization process of bottled milk is studied and the influence of the way to place the bottle inside the oven for a heating period is addressed [17]. However, the analysis of thermal process in the

pharmaceutical industry is keen to be studied regarding containers, such as vials and needle cylinders. As the temperature elevating process differs from material to material, the drying and sterilization process of the containers requires specific calculation.

- There are some studies that look into the numerical analysis of sterilization ovens. For instance, several structure improvements of sterilization ovens have been proposed with considerable simulation results after CFD regarding uniformity of airflow inside the oven [18-20]. However, from industrial perspective, the practical validation of equipment is missing which limits the structure improvement methods to be applied to practical use due to the equipment validation requirement from sterilization process validation, according to Current Good Manufacture Practices (cGMPs). Moreover, the oven-like sterilization equipment in these studies are usually considered as batch-based production equipment rather than continuous production equipment, also known as tunnel-like equipment. The airflow is more independent from heat distribution in oven-like equipment and is more predictable, while the heat distribution and airflow in tunnel-like equipment are mutually dependent with strong dynamics.
- There are other studies that look into the heat transfer process of preparation containers. Vials are considered as a porous medium for overall numerical calculation, which loses the individual vial's heating curve [21]. The temperature elevation process of an individual vial [22] and a single batch of asparaguses in a still can [23] are respectively studied to obtain their heating curve prediction. Wang's research [22] reveals the airflow distribution inside a depyrogenation tunnel using a two-dimensional model. The mentioned results are obtained via a series of simplification models, which cannot reflect the temperature and airflow three-dimensional distribution inside the depyrogenation tunnel.

From the analysis above, the bottleneck issue of this area is identified as the strong dynamics from pharmaceutical industry applications compared to impaired dynamics after mathematical modelling and control, leading to solutions of desired simulation results with less reliable consequences. Therefore, in order to validate the designed control system coping with the industrial applications from the purpose of cGMPs, current on-site equipment, a depyrogenation tunnel, is specially adopted for computational research through geometric modelling, meshing and irrelevance validation.

3. COMPUTATIONAL MODELLING

The hot air circulation sterilization method is normally used in the dry heat sterilization depyrogenation tunnel, as shown in Fig. 1. Here the typical equipment is adopted for the following geometric modelling and simulation calculation, with its detailed description found in previous work [3].

In this research, a geometric model is constructed via Catia V5R20, making use of its powerful surface modelling. Catia V5R20 is widely-used in design of vehicles and aerospace fields, but yet to be adopted in plant equipment design and analysis. Regarding numerical simulation of fluid, it is calculated via ANSYS 17.0, a large-scale general-purpose finite element analysis software with abroad application internationally.

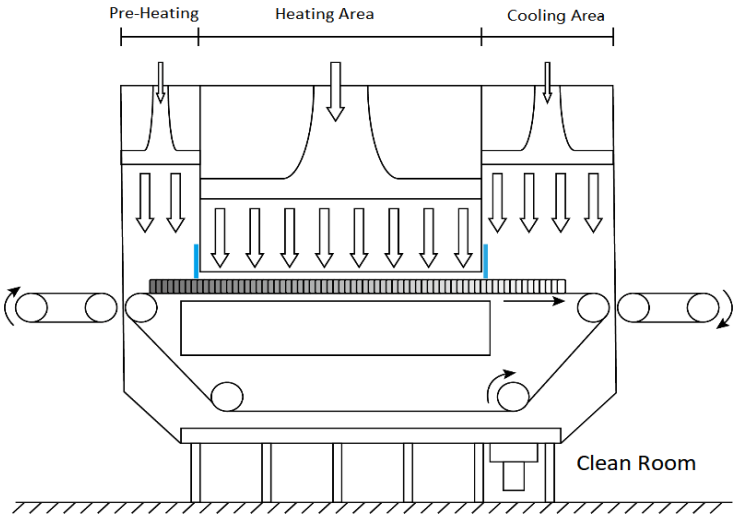

Fig. 1 Schematic Diagram of Depyrogenation Tunnel

3.1. Geometric Modelling

As shown in Fig. 2, the overall structure of the depyrogenation tunnel is mainly composed of heaters, inlet air pipes, induced draft fan, fan runner, air hood, high efficiency filter, drying chamber. The part structure is specifically modeled as shown in Fig. 3.

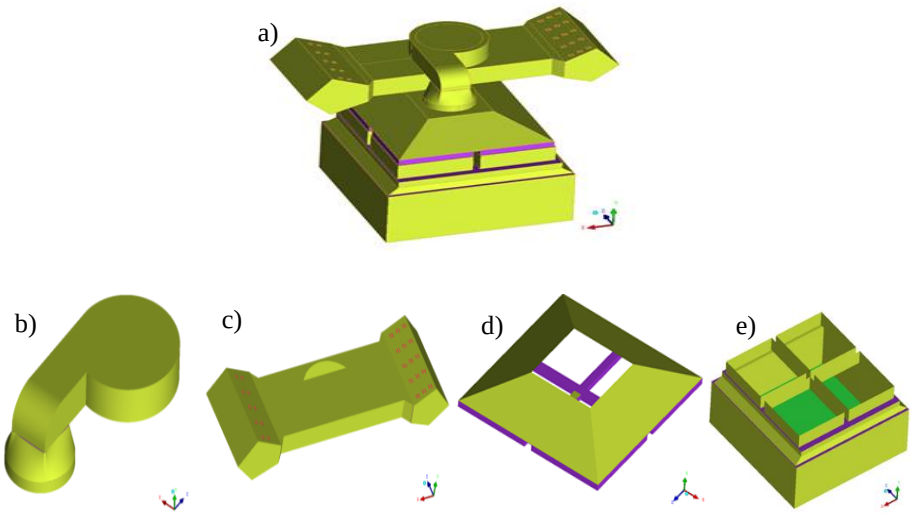

Fig. 2 a) Overall structure of the tunnel b) Heating tube area, c) Induced draft fan, d) Filter and drying chamber, e) Air hood

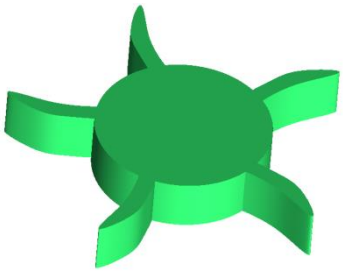

Fig. 3 Composition structure of the tunnel - Impeller

During the high-temperature sterilization process of the hot air circulation equipment, the hot air firstly is pumped from both sides of the heating pipe and heated from 300℃ to 350℃ by the heater, and the air flows through the hood are filtered to remove dust particles via a group of high-temperature-tolerant filters. The purified hot air enters the drying room to sterilize the vials at high temperatures. Afterwards, the hot air re-enters the heater through the return air duct and is heated again, so that the process of hot air circulation is completed. Meanwhile, part of the energy is lost during heat exchange between the circulating hot air and vials; while the temperature of hot air is lowered, it is still much higher than the room temperature. Thus, during the reheating process, the heating tube will heat the air to the required temperature by the tunnel with less energy, so as to achieve the purpose of energy saving.

The heat source structure in the heating tube area is defined as: a cylinder with a diameter of 14 mm and height of 200 mm. Sixty heating rods are determined and distributed on each side, then the total number of heating rods is 120. The air inlet surface is chosen rectangular, with a size of 754 mm*247.5 mm. The rotational speed of the induced draft fan impeller is set as 3000 rpm. It is worth mentioning that these specifications defined here mainly facilitate calculation and modeling, rather than the exclusive specification for the tunnel.

3.2. Mathematical Modelling

The sterilization process is in the middle of the continuous production line which is not a sealed container. Therefore, the airflow inside the tunnel is considered as incompressible flow, and it complies with the continuity Equation and Momentum Equation. During the flowing process of air flow, the convective heat transfer and conduction heat transfer are considered, through which energy conservation is satisfied. Considering the power of heat source is rather low, heat conduction through thermal radiation plays a far less significant role and is omitted. Therefore, the analysis is conducted based on continuity equation, momentum equation and energy equation respectively as follows.

3.2.1. Continuity Equation

All fluid motion problems must comply with the law of conservation of mass, that is, within a unit of time, the mass of the in-flowing fluid and the mass of the out-flowing fluid remains the same. In other words, the net inflow fluid mass is zero. According to this principle, the mass conservation equation is obtained as:

$$\frac{\partial \rho}{\partial \mathrm{t}}+\frac{\partial(\rho u)}{\partial x}+\frac{\partial(\rho v)}{\partial y}+\frac{\partial(\rho \mathrm{w})}{\partial \mathrm{z}}=0 \tag{1}$$

3.2.2. Momentum Equation

The momentum equation is also known as the Naiver-Stokes equation, which can be described as: the rate of change of the momentum of the fluid with time was equal to the sum of various external forces acting on the fluid. The flow rate, viscosity, density, humidity and other index changes of the micro-element are included by the Naiver-Stokes expression, which all vary over space and time.

$$\frac{\partial(\rho u)}{\partial t}+\operatorname{div}(\rho u \boldsymbol{u})=-\frac{\partial p}{\partial x}+\frac{\partial \tau_{xx}}{\partial x}+\frac{\partial \tau_{yx}}{\partial y}+\frac{\partial \tau_{zx}}{\partial \mathrm{z}}+F_x \tag{2}$$

$$\frac{\partial(\rho v)}{\partial t}+\operatorname{div}(\rho v \boldsymbol{u})=-\frac{\partial p}{\partial y}+\frac{\partial \tau_{xy}}{\partial x}+\frac{\partial \tau_{yy}}{\partial y}+\frac{\partial \tau_{zy}}{\partial \mathrm{z}}+F_y \tag{3}$$

$$\frac{\partial(\rho w)}{\partial t}+\operatorname{div}(\rho w \boldsymbol{u})=-\frac{\partial p}{\partial z}+\frac{\partial \tau_{xz}}{\partial x}+\frac{\partial \tau_{yz}}{\partial y}+\frac{\partial \tau_{zz}}{\partial \mathrm{z}}+F_z \tag{4}$$

where: ρ - density of air, t - fluid flow time, u, v, ω - velocities of the micro-element along the x, y, and z coordinate axes respectively, F_x, F_y, and Fz are the sum of various external forces in total along the x, y and z coordinate axes respectively.

3.2.3. Energy Equation

According to the energy equation of fluid dynamics, the growth rate of energy in the micro-element is equal to the net heat entering the micro-element and the total work done by the surface force and physical force on the micro-element. Thus, the energy conservation expression is obtained as:

$$\frac{\partial(\rho T)}{\partial t}+\operatorname{div}(\rho \boldsymbol{u} T)=\operatorname{div}[\frac{h}{c_p} \bullet \operatorname{grad} T]+S_T \tag{5}$$

where: T - thermodynamic temperature, c_p - specific heat capacity h - heat transfer index of the fluid S_t - internal heat source of the fluid.

The part where the mechanical energy of the fluid is converted into heat due to the viscous effect, which is referred to as the viscous dissipation term for short. In order to construct closure equations to describe the flowing process and heat transfer equations, a state equation is introduced as Eq. (6):

$$p=p(\rho, T) \tag{6}$$

In terms of ideal gas, the equation of state is:

$$p=\rho R T \tag{7}$$

where the molar gas constant is denoted by R.

3.2.4. Turbulence Modelling

The standard k - ε turbulence model is adopted for numerical simulation according to the air flow in the tunnel. ε that represents the dissipation rate in the model is defined as:

$$\varepsilon = \frac{\mu}{\rho}\left(\frac{\partial u_i^{'}}{\partial x_k}\right)\left(\frac{\partial u_i^{'}}{\partial x_k}\right) \tag{8}$$

Here μ_t - turbulent viscosity can be expressed as a function of k and ε as follows in specific:

$$\mu_t = \rho C_\mu \frac{k^2}{\varepsilon} \tag{9}$$

In the standard k-ε turbulence model, k and ε represent two fundamental unknowns, and their corresponding transport equations are as follows [24]:

$$\frac{\partial(\rho k)}{\partial t} + \frac{\partial(\rho k u_i)}{\partial x_i} = \frac{\partial}{\partial x_j}\left[\left(\mu + \frac{\mu_t}{\sigma_k}\right)\frac{\partial k}{\partial x_j}\right] + G_k + G_b - \rho\varepsilon - Y_M + S_k \tag{10}$$

$$\frac{\partial(\rho\varepsilon)}{\partial t} + \frac{\partial(\rho\varepsilon u_i)}{\partial x_i} = \frac{\partial}{\partial x_j}\left[\left(\mu + \frac{\mu_t}{\sigma_\varepsilon}\right)\frac{\partial \varepsilon}{\partial x_j}\right] + C_{1\varepsilon}\frac{\varepsilon}{k}(G_k + C_{3\varepsilon}G_b) - C_{2\varepsilon}\rho\frac{\varepsilon^2}{k} + S_\varepsilon \tag{11}$$

where: C_μ, $C_{1\varepsilon}$, $C_{2\varepsilon}$, $C_{3\varepsilon}$ - empirical constants, G_k - generation term of the turbulent dynamic energy caused by the average velocity gradient, k - turbulent dynamic energy, G_b - generation term of turbulent dynamic energy caused by buoyancy, Y_M - contribution of pulsation expansion in compressible turbulence, δ_k, δ_t - prandtl numbers corresponding to k and ε respectively, S_k, S_ε - user-defined source items.

4. MESH GENERATION AND BOUNDARY CONDITIONS

The realization of the tunnel mesh is generated by ANSYS ICEM CFD software. The mesh generated by ANSYS is an unstructured mesh type, with all tetrahedral elements. In order to ensure the accuracy and reliability of the calculation, the detailed structures such as the impeller of the induced draft fan and the heating pipe are subjected to mesh refinement processing, as shown in Fig. 4. In order to study the influence of the number of meshes on the calculation results, a total of five different numbers of meshes were distinguished, 2.32 million, 3.45 million, 5.69 million, 6.05 million and 6.77 million of meshes, respectively. Subsequently, for the above five mesh schemes, mesh independence test calculations were performed. The value of empirical constants are as follows: $C_{1\varepsilon}$=1.44, $C_{2\varepsilon}$=1.92, $C_{3\varepsilon}$=1.0, C_μ=0.09, σ_k=1.0, σ_ε=1.3.

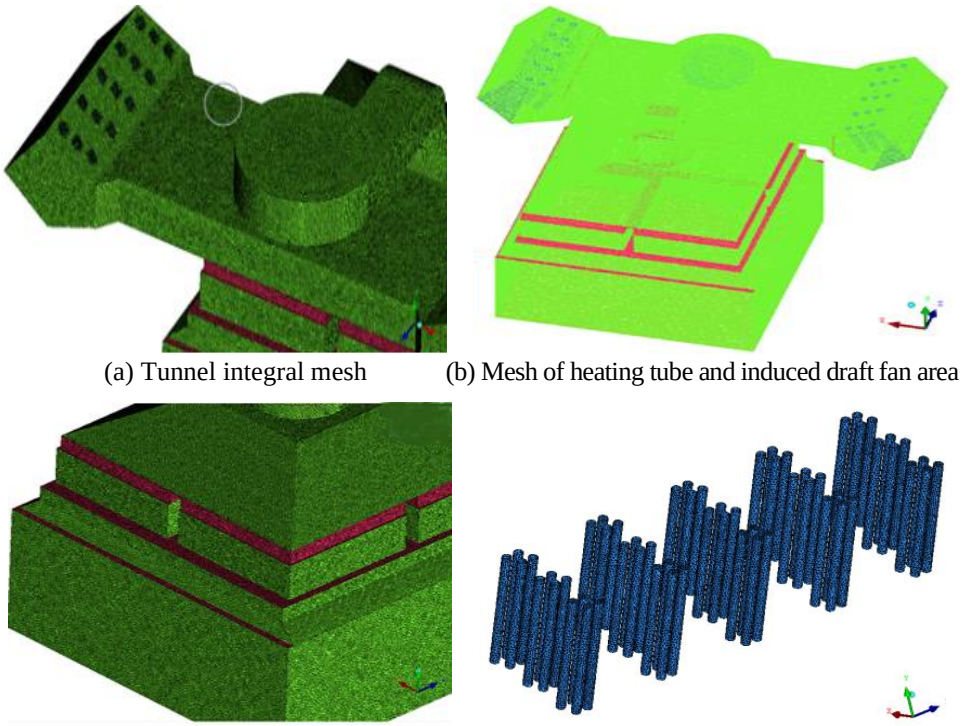

(a) Tunnel integral mesh (b) Mesh of heating tube and induced draft fan area

(c) Heating tube mesh (d) Mesh of filter and drying chamber

Fig. 4 Tunnel meshing

As mentioned previously, the standard *k-ε* turbulence model is adopted for calculations. The inlet of the tunnel adopted the speed inlet boundary condition, with the speed of 4.2 m/s, the inlet temperature of 573 K, the impeller speed of the induced draft fan was 3000 rpm, and the rotation direction of the induced draft fan is along the positive Y axis. In terms of outlet pressure, the outlet boundary condition is used, with relative pressure zero. The entire outer wall of the tunnel is set as the adiabatic boundary condition; the heating tube is set as the constant heating surface, with the heating density of 350 W/m^2. The solution is based on the pressure-velocity coupled simple algorithm, and the pressure and momentum are discretized by adopting the second-order upwind scheme.

In the calculation, the fluid medium is hot air and the solid material is considered as borosilicate glass. According to the theory of heat transfer, temperature has a significant influence on air density and thermal conductivity. Consequently, when setting the air physical property parameters, the corresponding polynomials are fitted and obtained according to their changing laws with temperature, as shown in Table 1 as below.

Table 1 Physical Parameters and Expressions [25]

Physical parameters	Expression
Density (kg/m^3)	$\rho = 2.836 - 0.008T + 1.055\times10^{-5}T^2 - 4.841\times10^{-9}T^3$
Thermal conductivity (W/(m·k))	$\lambda = 0.003 + 8.314\times10^{-5}T - 2.105\times10^{-8}T^2$

The above boundary conditions were used for the mesh independence verification of the tunnel structure, and the same boundary conditions and parameters were used for the calculation. The results of different mesh numbers were obtained by calculation, as shown in Table 2. According to the comparison of the average velocity of the outlet surface, when the number of meshes increased from 2.32 million to 5.69 million, the average speed of the outlet surface decreased from 3.9795m/s to 3.697m/s. When the number of meshes reached 6.05 million, the error between the calculation result of the mesh and the calculation result of the mesh number of 5.69 million was 0.54%. Continued increases in the number of meshes had less effect on the average velocity of the outlet surface. The variation trend between the number of meshes and the average velocity of the outlet surface is shown in Fig. 5. Taking into account a variety of cost factors, namely, the accuracy and reliability of the calculation, computing resources and computing time, the mesh with the final mesh number of 6.05 million was selected as the final calculation scheme, and this mesh scheme was adopted for subsequent calculations.

Table 2 Calculation results of mesh independence verification

Number of meshes (10,000)	Average speed of outlet surface (m/s)	Relative error	Average temperature at the outlet surface (K)
232	3.9795	-	574.800
345	3.9235	1.41%	574.798
569	3.6970	5.77%	574.778
605	3.7169	0.54%	574.798
677	3.7594	1.14%	574.789

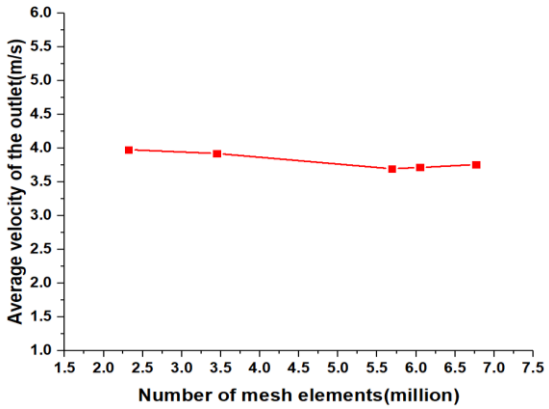

Fig. 5 Variation relationship between the number of meshes and the average velocity of the outlet surface

5. Results and Analysis

5.1. Results Analysis

Verified by mesh independence, the final mesh size of 6.05 million was deduced. The outer wall of the heating tube was fully set as a constant heating surface, with the heating density of 350 W/m^2. According to this mesh, the steady-state numerical simulation calculation was carried out, and the final distribution of the flow field and temperature field inside the tunnel was obtained as follows.

Fig. 5 shows the overall pressure and temperature distribution of the tunnel, and it can be observed that the heating area and the outer wall of the induced draft fan show obvious high pressure areas, while the wind hood turned up in the drying room, obvious low pressure areas.

There is an apparent thermal plume phenomenon on the wall near the heating tube area, mainly because the heating tube was a constant heating component, which had a relatively obvious heating effect on the heating area. Driven by the inlet airflow, the heat generated a thermal plume as shown in Fig. 6.

According to GMP requirements to equipment with sterilization purpose, the airflow inside the tunnel for sterilization is expected as laminar. From Fig. 6, considering the cross infection issue especially in pharmaceutical industries, such wind hoods are expected to be optimized in the following design.

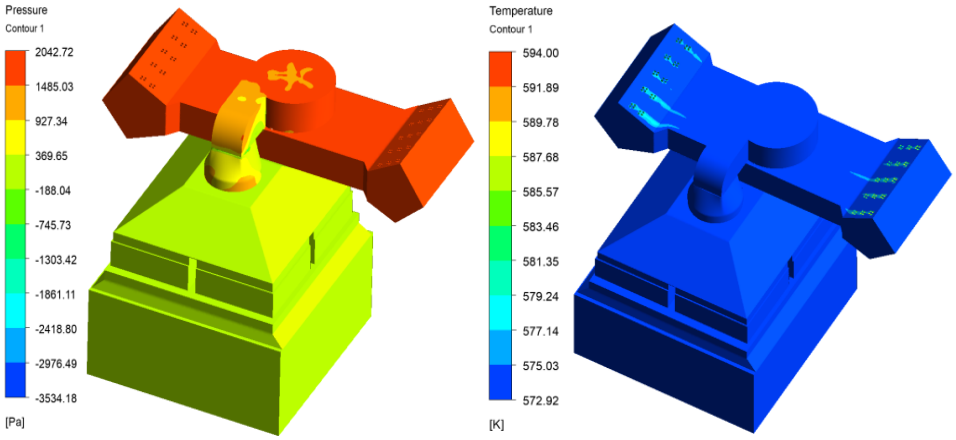

(a) Pressure (b) Temperature

Fig. 6 Distribution of the overall pressure and temperature of the tunnel

Fig. 7 shows the streamline distribution of the airflow inside the tunnel. The airflow flowed into the impeller and the induced draft fan channel through the inlet of the tunnel, formed a relatively high-speed distribution because the rotation of the impeller part increased the airflow velocity. After coming out of the induced draft fan channel, most of the accelerated airflow was discharged from the center of the drying chamber directly, with a large discharge speed; another part of the air flow generated a low-speed vortex in the area near the wall of the drying chamber. The airflow in this part was comparatively turbulent. According to the phenomenon that vials

next to the tunnel surface would fall down occasionally and cause long-time shutdown identified in the previous study [4], this result gives a reasonable explanation.

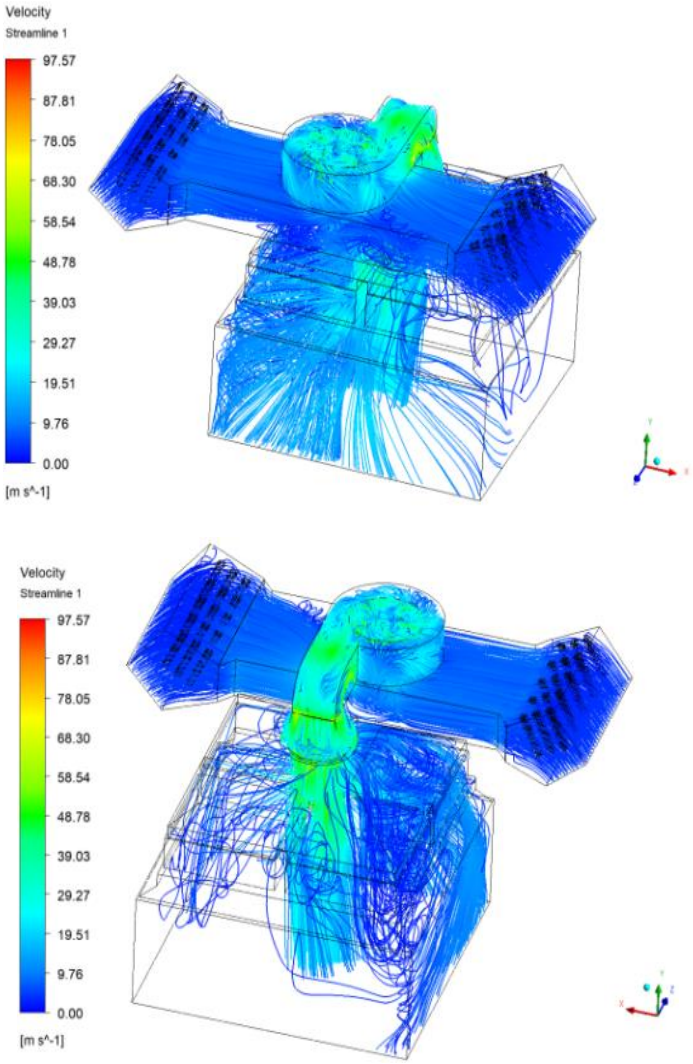

Fig. 7 3D streamline distribution of the front and reverse sides of the tunnel: a) Front size; b) Reverse side

The flow field and temperature field distribution of section X=0.683 m were shown in Fig. 8. The temperature distribution inside the drying chamber was significantly higher than in other areas. However, due to the relatively low flow rate of air flow in the drying chamber, the airflow generated vortices of different sizes inside the hood and the drying chamber, which contributes to the drying effect to a certain extent.

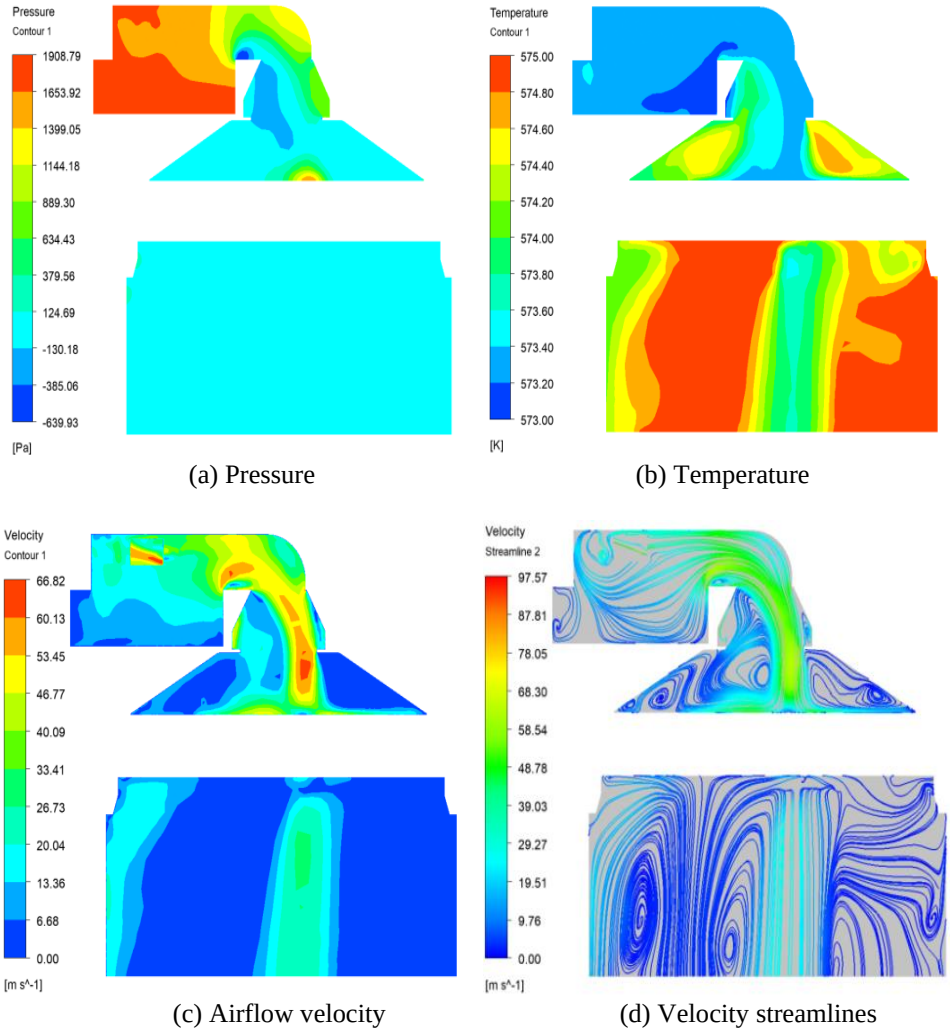

(a) Pressure (b) Temperature

(c) Airflow velocity (d) Velocity streamlines

Fig. 8 Flow field and temperature field distribution of section X=0.683 m

The flow field and temperature field distribution of section Z=-0.687 m were shown in Fig. 9. The temperature near the center line of the drying chamber was relatively low, while the temperature near the wall surface was relatively high. The major reason was that the airflow velocity near the centerline of the drying chamber was relatively large, and the convective heat transfer effect of the space was prominent, and the heat was carried away by the airflow, resulting in a comparatively low temperature in this area. To a certain extent, the uneven temperature distribution inside the drying chamber was caused by the low-speed vortex generated inside the drying chamber. Therefore, it was necessary to optimize and improve the design of the internal structure of the drying chamber subsequently.

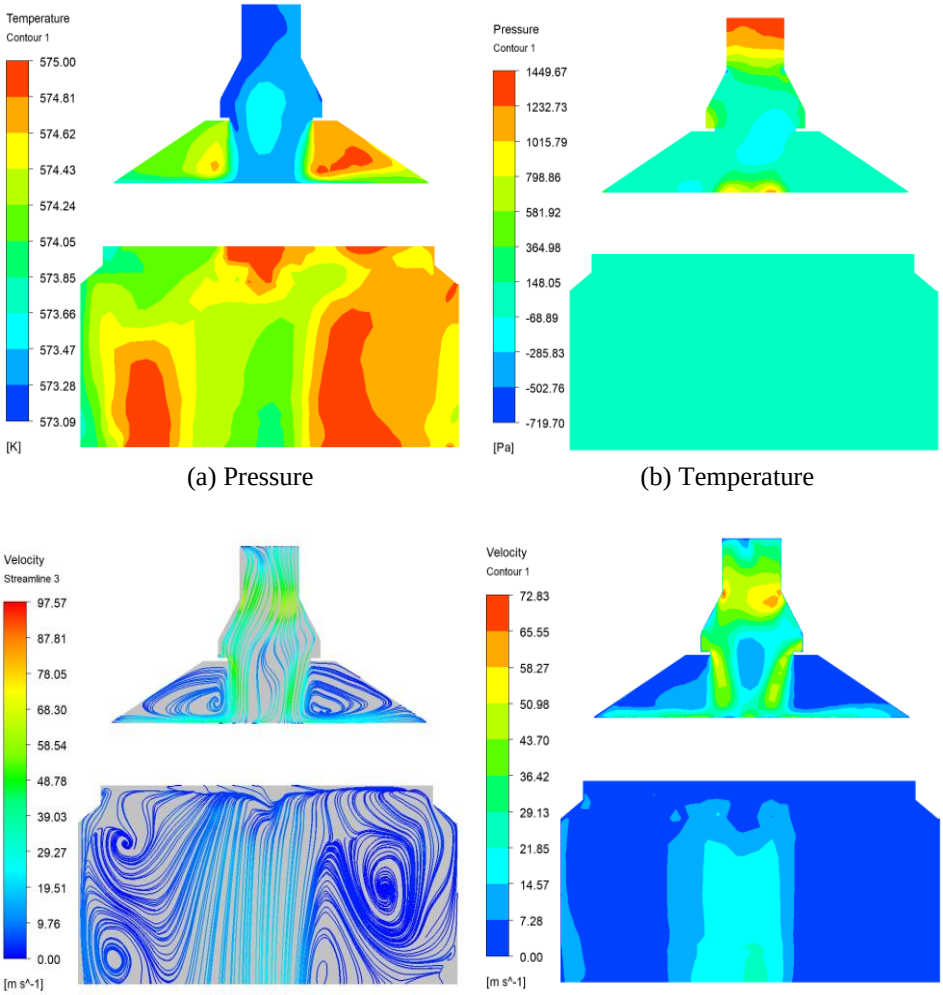

(a) Pressure (b) Temperature

(c) Airflow velocity (d) Velocity streamlines

Fig. 9 Flow field and temperature field distribution of section Z=-0.687 m

Fig. 10 has shown the velocity and temperature distribution on the outlet surface of the tunnel under the condition that the inlet velocity was 4.2 m/s. The results suggest that the temperature and airflow velocity distribution on the outlet surface of the tunnel was not uniform. Compared to the inlet temperature of 573 K, the average temperature at the outlet side was about 575 K, and the temperature rise was about 2°C. Most of the air flowed out directly from the center of the tunnel, resulting in uneven distribution of velocity and temperature at the center of the outlet surface.

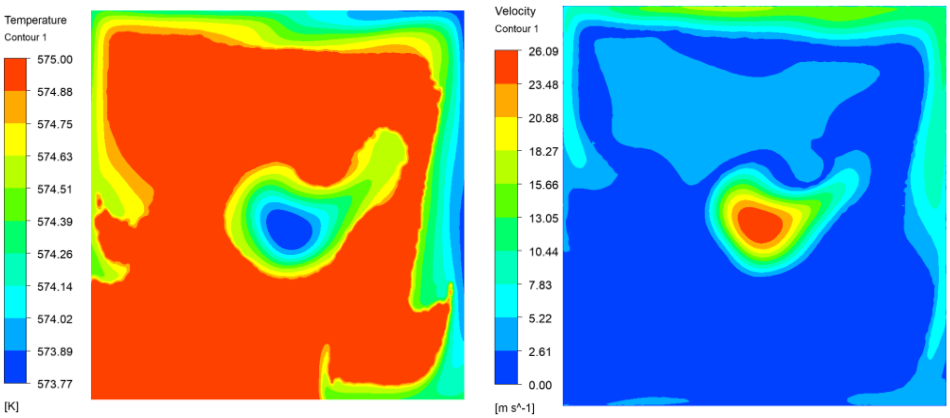

(a) Temperature (b) Airflow velocity

Fig. 10 Velocity and temperature distribution of outlet surface

By changing the inlet velocity of the tunnel, the inlet velocity was set to 6 m/s and 8 m/s respectively, while keeping the boundary conditions of other walls unchanged, and the numerical simulation calculation of the flow field and temperature field of the entire tunnel was performed. So as to explore the variation law of airflow velocity, temperature and pressure inside the drying chamber at different positions, the inner center line of the drying chamber was selected, and the variation data of the airflow velocity, temperature and pressure on the center line with the position were extracted and studied. The specific results were shown in Fig. 11.

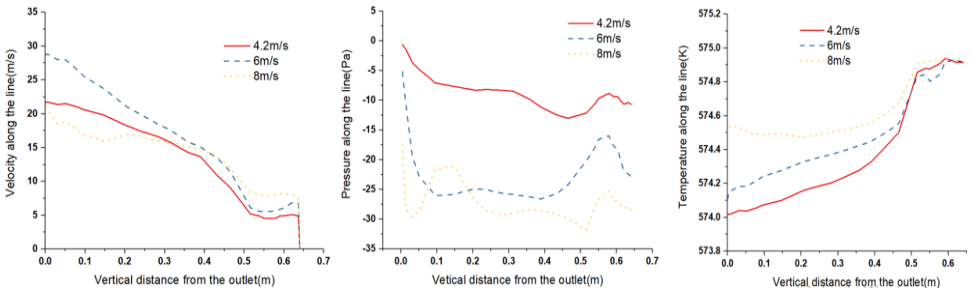

(a) Airflow velocity (b) Pressure (c) Temperature

Fig. 11 Variation law of airflow velocity, pressure and temperature on vertical centerline of drying chamber

It can be concluded from Fig. 11 that under different inlet speed conditions, the farther away from the outlet, the lower the airflow velocity on the centerline, displaying a definite trend; the relative pressure changes on the entire centerline are basically the same, and the overall relative pressure is almost zero. The temperature on the centerline shows an increasing trend with the distance from the outlet, which is mainly because the farther away from the outlet, the smaller the airflow velocity, the less obvious the heat transfer effect, and the greater the temperature of the space.

5.2. Results Validation Discussion

Under most circumstances, the errors of computational results are caused by discretization, namely the discretization error, which is caused by mesh numbers. In this research, firstly the calculation results of mesh independence verification as shown in Table 2 removes the influence of mesh numbers from computational results. Secondly, the average temperature at the outlet surface regarding different mesh numbers are very close, which is 574.8K (recorded in Table 2), indicating the steady state of computation results. Considering the boundary conditions are measured from practical equipment, the results are proved with accuracy and reliability.

6. CONCLUSIONS

In this research, the tunnel is modeled geometrically using Catia and 5 numbers of unstructured meshes, 2.32 million, 3.45 million, 5.69 million, 6.05 million and 6.77 million respectively, are generated using ANSYS. The generated meshes are verified by mesh independence, and the number of computing grids is determined to be 6.05 million finally. Considering that the constant heating density of the heating tube was 350 W/m2, when the inlet velocity is 4.2 m/s, 6 m/s and 8 m/s respectively, the corresponding steady flow field and temperature field inside the tunnel are calculated, thus, the following basic conclusions are ultimately summed up as below:

- After entering the tunnel from the inlet, most of the airflow is discharged from the center of the drying chamber directly, with a large discharge speed; another part of the air flow generated a low-speed vortex in the area near the wall of the drying chamber. The airflow in this part was comparatively turbulent.
- Inside the drying chamber, low-speed vortices of different intensities are generated, and the temperature in the center is relatively low, while the temperature close to the wall is relatively high.

Although the depyrogenation tunnel structure and its heating and sterilization process is studied using a CFD method in this research, many problems remained to be improved and solved in the future research, which include:

- Structure improvement to reduce the low-speed vortex

In this study, the low-speed vortex in the area near the wall of the drying chamber is identified, which is in line with the empirical results that vials occasionally fall down, causing an unexpected shutdown of production line. In the future work, the structure inside of the tunnel can be improved to decrease the vortex. Furthermore, GMP requirements should be considered when performing structure improvement.

- Time-variant calculation

In this study, the steady-state temperature and fluid flow fields are calculated using CFD methods. However, the temperature field inside the tunnel is time-variant, taking especially the continuous production process in consideration. Therefore, in the following study time-variant calculation could be conducted to express the dynamic process along time.

- Control system optimization for energy saving

In this study, the modelling and CFD calculation is carried out in terms of the depyrogenation tunnel to validate the air fluid field and temperature field results. According to the uneven distributed temperature from the wall to the central line, the reference input (temperature) of the control system could be lower.

Acknowledgement: *This work was partly supported by the National Natural Science Foundation of China (No. 61803188), Open Fund Project of Fujian ProvincialKey Laboratory of Information Processing and Intelligent Control (Minjiang University) (Grant No. MJUKF-IPIC202204) and Research Foundation of Jinling Institute of Technology (No. jit-b-202029).*

REFERENCES

1. Huang, L., Zhou, Y., Wang, Y., Lin, M., 2021, *Optimization of S-Nitrosocaptopril Monohydrate Storage Conditions Based on Response Surface Method*, Molecules, 26(24), 7533
2. Krüger, O., Ebner, I., Kappenstein, O., Roloff, A., Luch, A., Bruhn, T., 2021, *Towards a better comparability during GMP assessment–Identifying the main parameters that influence the loss of volatile organic compounds from silicone elastomers*, Food Packaging and Shelf Life, 30, 100758
3. Wang, Y., Yang, Z., Gu, S., Chen, W., Yu, Z., 2021, *Research on pole placement approach of non-standard state space model with case study*, International Journal of Modelling, Identification and Control, 37(3-4), pp. 249-257.
4. Wang, Y., Zhu, Q., Nibouche, M., 2015, *State-space Modelling and Control of a MIMO Depyrogenation Tunnel*, 34th Chinese Control Conference, pp. 674-679.
5. Wang, Y., Zhu, Q., Nibouche, M., 2015, *Mamdani type controller design for MIMO systems with case study*, 2015 7th International Conference on Modelling, Identification and Control (ICMIC), IEEE, pp. 1-6
6. Komissarov, A.V., Bibikov, D.N., Badarin, S.A., Sinitsyna, N.V., Kostyleva, N.I., Ovchinnikova, M.V., Korovkina, G.I., Zinina, O.S., Plotnikov, I.A., Nikiforov, A.K., 2020, *Calculation of dependences for estimating the amount of weight loss during lyophilization of diagnostic preparations*, Proceedings of Universities, Applied Chemistry and Biotechnology, 10(3), pp. 506-514.
7. Boom, F., Le, B., Paul, P., Boehringer, S., Kosterink, J., Touw, D., 2021, *Improving the aseptic transfer procedures in hospital pharmacies part A: methods for the determination of the surface bioburden on ampoules and vials*, European journal of hospital pharmacy, Science and practice, 28 (1), pp. 38–41.
8. Gupta, S., Román-Ospino, A.D., Baranwal, Y., Hausner, D., Ramachandran, R., Muzzio, F.J., 2021, *Performance assessment of linear iterative optimization technology (IOT) for Raman chemical mapping of pharmaceutical tablets*, Journal of Pharmaceutical and Biomedical Analysis, 205, 114305
9. Hussain, S.M., Jamshed, W., 2021, *A comparative entropy based analysis of tangent hyperbolic hybrid nanofluid flow: Implementing finite difference method*, International Communications in Heat and Mass Transfer, 129, 105671
10. Yu, Z., Song, Y., Song, D., Liu, Y., 2021, *Spatial interpolation-based analysis method targeting visualization of the indoor thermal environment*, Building and Environment, 188, 107484
11. Gumbarević, S., Milovanović, B., Gaai, M., Bagarić, M., 2021, *Thermal transmittance prediction based on the application of artificial neural networks on heat flux method results*, Journal of Physics: Conference Series, 2069, 012152
12. Bel-Rhlid, R., Berger, R.G., Blank, I., 2018, *Bio-mediated generation of food flavors–Towards sustainable flavor production inspired by nature*, Trends in Food Science & Technology, 78, pp. 134-143.
13. Paton, J., Khatir, Z., Thompson, H., Kapur, N., Toropov, V., 2013, *Thermal energy management in the bread baking industry using a system modelling approach*, Applied Thermal Engineering, 53(2), pp. 340-347.
14. Khatir, Z., Paton, J., Thompson, H., Kapur, N., Toropov, V., 2013, *Optimisation of the energy efficiency of bread-baking ovens using a combined experimental and computational approach*, Applied energy, 112, pp. 918-927.
15. Khatir, Z., Taherkhani, A.R., Paton, J., Thompson, H., Kapur, N., Toropov, V., 2015, *Energy thermal management in commercial bread-baking using a multi-objective optimisation framework*, Applied Thermal Engineering, 80, pp. 141-149.
16. Tanthadiloke, S., Chankerd, W., Suwatthikul, A., Lipikanjanakul, P., Mujtaba, I.M., Kittisupakorn, P., 2016, *3D computational fluid dynamics study of a drying process in a can making industry*, Applied Thermal Engineering, 109, pp. 87-98.
17. Dhayal, P., Chhanwal, N., Anandharamakrishnan, C., 2013, *Heat transfer analysis of sterilization of canned milk using computational fluid dynamics simulations*, Journal of Food Science and Engineering, 3(11), 571
18. Ji, Z., 2019, *Discussion on improvement of hot air circulation oven*, Chemical Enterprise Management, 11, pp. 141–142.

19. Yu, M., Geng, Y., 2017, Study on uniformity of air supply in air duct of sleeper vehicle, Railway technical supervision, China, 45(1), pp. 41–43.
20. Wan, M., 2012, *Design and study of laminar hot air sterilization tunnel oven*, Master thesis, Shaanxi University of Science and Technology.
21. Wan, M.W., Zhang, S.H., 2012, *Numerical Simulation of the Tunnel Oven with Fluent Software*, Advanced Materials Research, 399, pp. 1856-1861.
22. Wang, B., Yu, Y., Lu, C., 2014, *Simulation of temperature rise curve of Celine bottle based on FLUENT*, Chemical and Pharmaceutical Engineering, 35(3), pp. 43-47.
23. Dimou, A., Yanniotis, S., 2011, *3D numerical simulation of asparagus sterilization in a still can using computational fluid dynamics*, Journal of Food Engineering, 104(3), pp. 394-403.
24. ANSYS, Inc, ANSYS FLUENT Theory Guide, 2012, 10 version 14.5, pp. 47-49.
25. Wang, Z., Zou, Y., Liu, B., Zhang, Z., 2020, *Flow Field Simulation and Structure Optimization of Hot Air Circulation Tunnel Oven*, Chinese Journal of Process Engineering, 20(5), pp. 531-539.